Cooperative Energy Transfer Controls the Spontaneous Emission Rate Beyond Field Enhancement Limits

Mohamed ElKabbash,[1,*] Ermanno Miele,[1,2] Ahmad K. Fumani,[1] Michael S. Wolf,[1] Angelo Bozzola,[2] Elisha Haber,[1] Tigran V. Shahbazyan,[3] Jesse Berezovsky,[1] Francesco De Angelis,[2] and Giuseppe Strangi[1,2,4,†]

[1]*Department of Physics, Case Western Reserve University, 10600 Euclid Avenue, Cleveland, Ohio 44106, USA*

[2]*IIT-Istituto Italiano di Tecnologia, via Morego 30, 16163 Genova, Italy*

[3]*Department of Physics, Jackson State University, Jackson, Mississippi 39217, USA*

[4]*CNR-NANOTEC Istituto di Nanotecnologia and Department of Physics, University of Calabria, 87036-Rende, Italy*

(Received 13 December 2018; published 22 May 2019)

Quantum emitters located in proximity to a metal nanostructure individually transfer their energy via near-field excitation of surface plasmons. The energy transfer process increases the spontaneous emission (SE) rate due to plasmon-enhanced local field. Here, we demonstrate a significant acceleration of the quantum emitter SE rate in a plasmonic nanocavity due to cooperative energy transfer (CET) from plasmon-correlated emitters. Using an integrated plasmonic nanocavity, we realize up to sixfold enhancement in the emission rate of emitters coupled to the same nanocavity on top of the plasmonic enhancement of the local density of states. The radiated power spectrum retains the plasmon resonance central frequency and line shape, with the peak amplitude proportional to the number of excited emitters indicating that the observed cooperative SE is distinct from superradiance. Plasmon-assisted CET offers unprecedented control over the SE rate and allows us to dynamically control the spontaneous emission rate at room temperature which can enable SE rate based optical modulators.

DOI: 10.1103/PhysRevLett.122.203901

Ordinary fluorescence arises from the decay of excited quantum emitters (QEs) to lower energy states by spontaneous emission (SE) where QEs interact independently with the radiation field. This interaction can be controlled by modifying the emitter's electromagnetic environment. The SE rate is directly proportional to the electromagnetic local density of states (LDOS) [1–3], i.e., the number of electromagnetic modes available for the emitter to radiate into per unit volume and frequency interval. LDOS can be modified by, e.g., placing an emitter inside a cavity. The cavity enhanced SE rate is proportional to the ratio of the cavity quality factor Q to modal volume V, known as the Purcell effect [3]. The emitters' SE rate has been significantly enhanced using plasmonic nanocavities (PNCs) supporting localized surface plasmon (LSP) modes [2–5]. The LDOS enhancement in a PNC results from strong field confinement within small plasmon mode volume, so a QE transfers its energy to a resonant plasmon mode with an energy transfer rate Γ^{ET} faster than the free-space SE rate [Fig. 1(a)]. Subsequently, a PNC acts as an optical antenna radiating transferred energy with a significantly faster rate due to its large size and dipole moment [2,6]. Accordingly, following the excitation of a QE, the emission rate is proportional to Γ^{ET}. However, the SE rate of an individual QE is restricted by ultimate limits on plasmonic field enhancement [7,8].

When an ensemble of QEs is coupled to a plasmonic structure, SE can be greatly accelerated by cooperative effects arising from plasmon-assisted correlations between QEs. For example, interactions of QE with common radiation field enhanced by resonant Mie scattering are predicted to lead to plasmon-enhanced superradiance characterized by SE rate proportional to the *full ensemble size* including both excited and ground-state QEs [10–14]. However, the plasmonic enhancement of radiation coupling is offset by relatively strong absorption, compared to scattering, in small metal structures [11], which inhibits coherence buildup that precedes the superradiance burst from incoherently excited emitters [15,16]. An observation of plasmon-enhanced superradiance, accordingly, remains challenging [17].

Conversely, strong plasmon absorption may lead to another cooperative effect in a system of N excited QEs coupled to a plasmonic resonator that does *not* require coherence buildup between excited QEs [9,18]. If plasmon frequency is tuned to resonance with QEs emission frequency, the indirect plasmonic coupling between QEs gives rise to collective states that transfer their energy to a plasmon *cooperatively* at a rate $\Gamma_c^{\mathrm{ET}} = \sum_i^N \Gamma_i^{\mathrm{ET}}$ where Γ_i^{ET} is the energy transfer rate of individual QEs [Fig. 1(b)]. Note that the Förster resonance energy transfer rate from QEs to a plasmon is determined by the spectral overlap between the donor (QE) emission band and the acceptor (plasmon) absorption band [19]. Since the plasmon spectral band is broader than that of QEs, the cooperative energy transfer (CET) rate is relatively insensitive, in contrast to

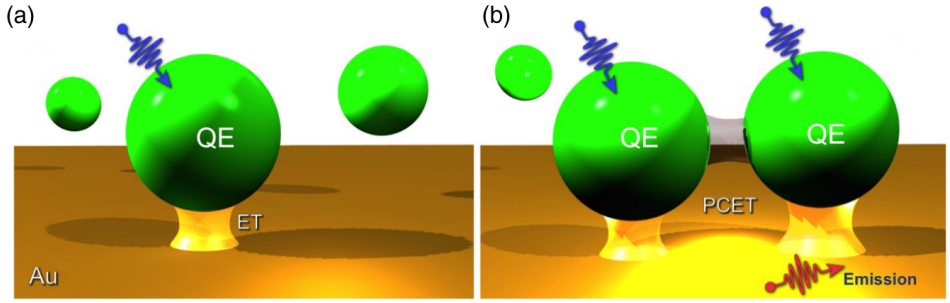

FIG. 1. (a) An excited QE coupled to plasmonic resonator non-radiatively transfers its energy, at a rate Γ^{ET} to the plasmon mode, which radiates it away. (b) An ensemble of QEs coupled to a resonant plasmon mode transfer their energy to it cooperatively at a rate Γ_c^{ET} that is the sum of individual rates [9].

superradiance [20,21], to natural variations of QEs emission frequencies, e.g., due to direct dipole coupling. Following CET to a plasmon mode, the possible energy flow pathways include (i) energy transfer from PNC to QEs, (ii) energy dissipation within PNC through Ohmic losses, and (iii) PNC antenna radiation. If the antenna's radiation efficiency is high, while the overlap between QEs' emission and absorption bands is relatively weak, the energy is mainly radiated away at approximately rate Γ_c^{ET}. Note that the values of individual rates Γ_i^{ET} are determined by the plasmon LDOS at the QEs' positions and can vary significantly depending on the system geometry [9,19]. However, if the LDOS does not change significantly in the region where QEs are distributed, Γ_i^{ET} are all comparable and the cooperative rate Γ_i^{ET} scales linearly with the number of excited emitters (N), hence the excitation power. Accordingly, the ensemble SE mediated by CET to plasmonic antenna can be controlled directly by the excitation power.

Here, we report the experimental observation of a cooperative SE from an ensemble of N excited QEs resonantly coupled to a PNC acting as a plasmonic antenna. We observe up to sixfold increase of the ensemble SE rate relative to the plasmonic LDOS enhancement which is linear in the excitation power. Simultaneously, the measured photoluminescence spectrum retains the plasmon resonance line shape while the overall emission intensity increases linearly with the excitation power. These observations imply that the radiation is emitted by the plasmonic antenna following CET from excited QEs [18]. The linear dependence of the ensemble SE rate on the number of excited QEs (as opposed to total number of emitters [21–23]) has not been observed previously. Such dependence as well as the incoherent nature of the CET mechanism [9,18] that does not require coherence buildup [15,16], in contrast to superradiance, provides a unique possibility for dynamically controlling the SE rate in the *same* electromagnetic environment by varying excitation power (see Supplemental Material [24], Note 2.1). We experimentally exploit CET to dynamically control the SE rate by modulating the excitation power, resulting in *reversible* increase and decrease of the SE rate at room temperature, which was only possible in previous works using complex photonic devices at cryogenic temperatures [31,32]. The cooperative enhancement of the ensemble SE rate takes place on top of the plasmon LDOS enhancement for individual emitter's SE rate paving the way towards SE rate control beyond field enhancement limits [7,8]. This is important for short-distance optical communication, to increase the modulation rate [6], and for optical data storage [33].

To demonstrate the effect, we fabricated three-dimensional hollow PNC [34,35] (Supplemental Material, methods [24]). Figures 2(a) and 2(b) show a SEM image of PNC array, and a single PNC cross section, respectively. The PNCs are composed of a cylindrical polymeric scaffold, 20 nm thick and 450 nm height, on which a 20 nm gold layer was conformally deposited. The geometry of the PNCs was chosen to ensure strong radiation directionality (Supplemental Material, Fig. S2 [24]). The radiation pattern from our PNC is highly directional and the large size of the PNC increases the antenna radiative efficiency [4,6,36] to ensure that the major energy pathway following energy transfer process is antenna radiation and that the collected photons are from antenna radiation. CdSe/ZnS quantum dots (QDs) were spin coated on the polymeric scaffold onto which the plasmonic shell is formed [Figs. 2(c) and 2(d)]. We chose QDs as our QEs over, e.g., fluorophores, as they have larger dipole moments which increases the nonradiative energy transfer efficiency [5], and exhibit relatively weak absorption in the photoluminescence frequency range to reduce reabsorption which is important to demonstrate CET (Supplemental Material, Fig. S3 [24]). The integrated PNC is designed such that QEs are at approximately the same distance away from the plasmonic shell to excite LSPs with the same energy transfer rate, i.e., $\Gamma_c^{ET} \approx N\Gamma^{ET}$ [Fig. 2(d)]. This relation is robust even for large fluctuations in QEs' positions since the LSP electric field inside PNC is nearly uniform. The PNC measured [Fig. 2(e)] and calculated [Fig. 2(f)] LSP resonance are in close agreement. To control for frivolous QD-metal interactions, we prepared a reference sample where the QDs were spin coated on an Au film. Figure 2(g) compares the QDs photoluminescence collected

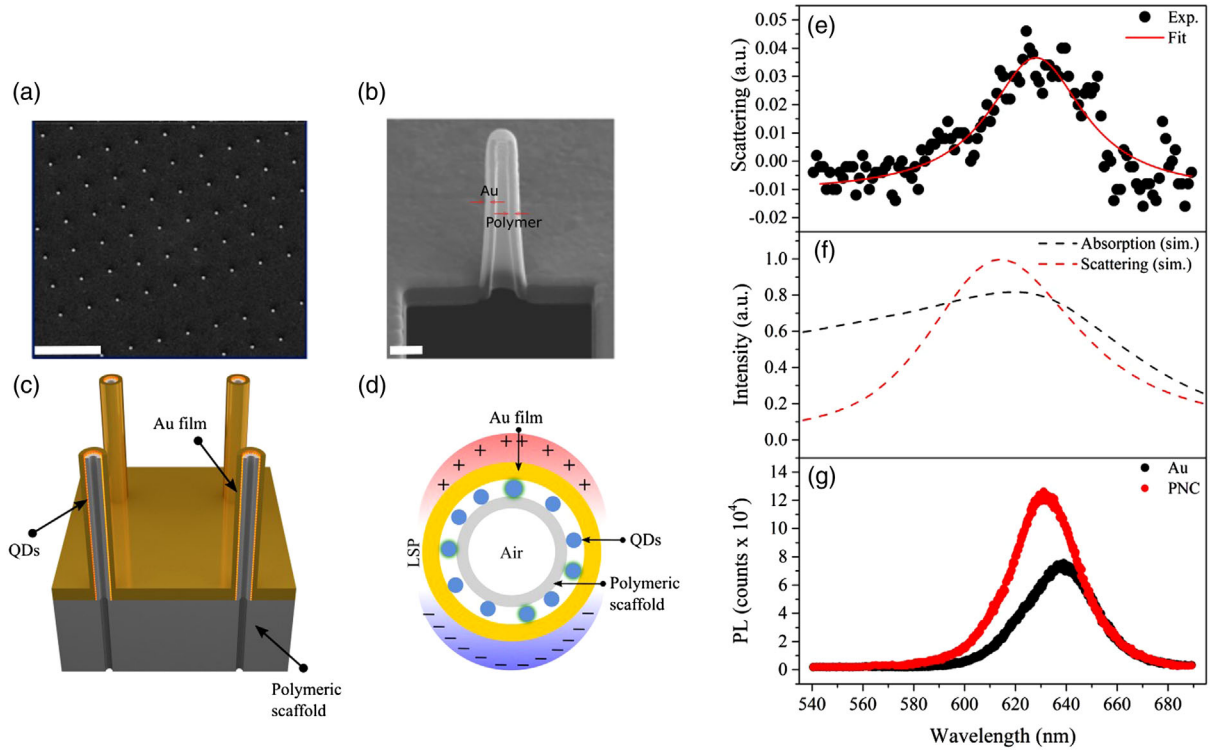

FIG. 2. (a) SEM image of plasmonic nanocavity (PNC) array (scale bar = 5 μm). (b) SEM image of a cross section of a single PNC that was cut using focused ion beam FIB (scale bar = 100 nm). (c) Schematic of the nanopillar PNC. The quantum dots (QDs) are spin coated on a polymeric scaffold, then an Au layer is deposited. (d) Schematic of a cross section of a single nanopillar. Incident light excites QDs that, subsequently, transfer their energy to excite localized surface plasmons (LSPs) which decay into a photon. (e) Measured scattering for PNC array; the resonance maximum was determined by fitting the data with a Lorentzian function. The measured resonance closely agrees with the calculated absorption and scattering presented in (f). (g) The photoluminescence of QDs spin coated on an Au film vs QDs incorporated in a single PNC.

from a single PNC and from the reference sample with excitation wavelength 490 nm and intensity 18.5 W/cm^2. The photoluminescence maximum is blueshifted from 638 (reference) to 631 nm (PNC) towards the LSP resonance peak (~628 nm) [37]. The blueshift in the photoluminescence maximum and the high directionality and radiative efficiency of our PNC ensure that collected photoluminescence is mainly from the nanoantenna due to excitation of LSPs [36,37] (Supplemental Material, Fig. S4 [24]).

Figure 3(a) shows the time-resolved photoluminescence from a single PNC and the reference Au film for different pump intensities (3.7–74 W/cm^2) and 490 nm excitation wavelength (Supplemental Material [24]). The reference sample measured lifetime shows no changes upon increasing the excitation intensity. Conversely, the PNC photoluminescence lifetime strongly depends on the excitation intensity. We fitted the photoluminescence decay curves with biexponential functions obtaining two characteristic decay times: a fast (slow) SE rate due to a short (long) living state, as shown in Fig. 3(b). It is known that CdSe/ZnS quantum dots have fast and slow SE rate components (Supplemental Material, Note 2.5, and Fig. S5 [24]) [38]. By increasing the pump intensity, the SE rates increased linearly up to sixfold for the PNCs, while no changes were measured for the Au film, as shown in Fig. 3(b). This linear dependence of the SE rate on the excitation intensity, accompanied by linear increase of the photoluminescence, is a clear signature of a plasmon-mediated CET. It is important to note that the QDs in both the PNC and the reference samples are subjected to comparable excitation conditions (Supplemental Material, Figs. S6 and S7 [24]).

The demonstrated dynamic control of QEs' SE rate in real time and at room temperature presents a significant challenge as it requires modifying the LDOS at a rate faster than the QEs SE rate (~1 GHz). The ability to do so would enables multiplexing in optical communication and modulation of lasers. Recent works dynamically controlled the fluorescence lifetime of QEs at cryogenic temperatures by controlling the radiation field in real time [31] or by modifying the exciton-cavity coupling strength [32]. Instead, CET mechanism provides real-time, room temperature, control over the SE rate through varying the number of QEs participating in CET. Figure 3(c) shows reversible dynamic control over the SE rate by varying the excitation intensity. Regions with white background represent data taken when the excitation intensity decreased from 37 to 4.4 W cm^{-2}, whereas light-blue regions represent data taken by increasing the excitation intensity from 4.4 to

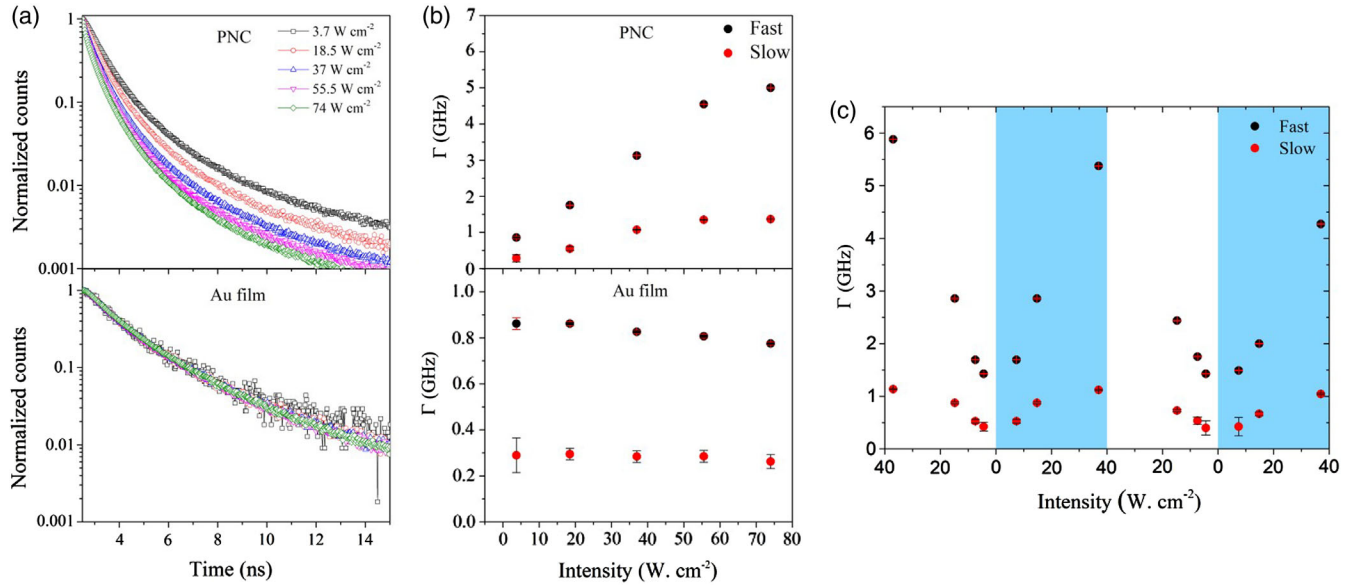

FIG. 3. (a) Measured time-resolved photoluminescence for five different excitation intensities for the PNC (top) and the reference Au film (bottom). The SE lifetime is intensity dependent only for the PNC. (b) The fitted SE rate fast component (black spheres) and slow component (red spheres) for the PNC (Top) and for the reference Au film (Bottom). (c) Reversible, dynamic control over SE rate. The fast and slow SE rate components vary by modifying N. The SE rate is linearly proportional to the excitation intensity.

37 W cm^{-2}. This reversible response offers a complete control on the SE rate and establish the basis for a novel class of optical modulators. Note that in the fourth region, the SE rates are slightly lower for all intensities. This is due to QDs bleaching over long exposure times which decreases N, hence, the CET rate.

To quantitatively demonstrate that the linear dependence of the measured SE rate is due to CET, we first investigate the origin of the fast (Γ^{fast}) and slow (Γ^{slow}) SE rates. Figure 4(a) shows the ratio ($\Gamma^{\text{fast}}/\Gamma^{\text{slow}}$) of QDs on the reference Au film as a function of intensity is ~3 suggesting that the fast and slow rates correspond to emission of charged biexcitons and charged excitons, respectively, according to the statistical scaling law at room temperature [38]. This is because a charged biexciton (3 electrons and 2 holes) have six decay pathways via electron-hole recombination, while a charged exciton (2 electrons and 1 hole) has only two decay pathways [Fig. 4(a) inset], (Supplemental Material [24], note 2.7). The SE rate of a QD coupled to a large nanoantenna is $\sim\Gamma^{\text{ET}}$. Accordingly, the same statistical scaling applies to energy transfer rates, i.e., $\Gamma^{\text{fast}}_{\text{ET}}/\Gamma^{\text{slow}}_{\text{ET}} \sim 3$. Below the saturation intensity, the number of excited QDs participating in CET scales linearly with the excitation intensity I with a scaling factor α, i.e., $N = \alpha I$ (since excited QDs' number is an integer, N here is understood as its average over a small intensity range).

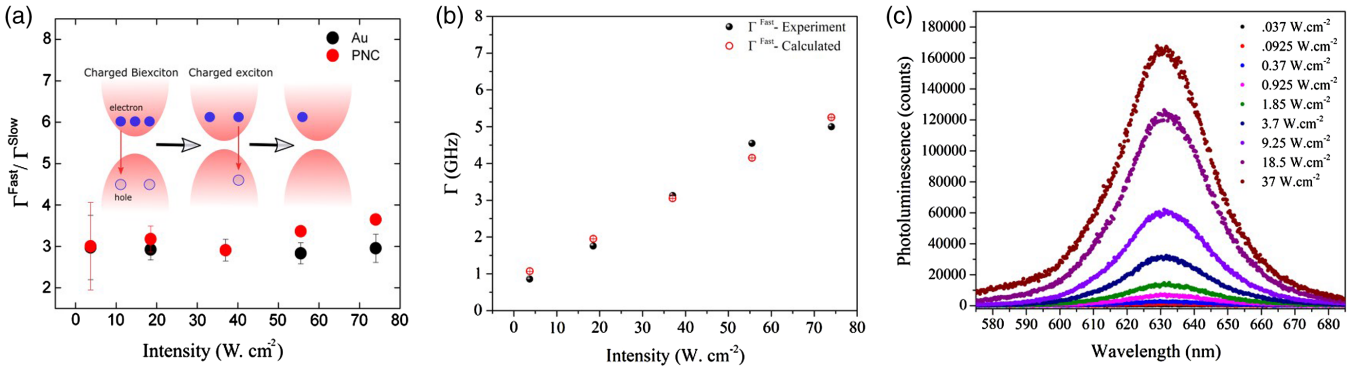

FIG. 4. (a) The ratio of the measured fast Γ^{fast} and slow Γ^{slow}SE rates for QDs on the reference Au film and inside the PNC. The ratio $\Gamma^{\text{fast}}(I)/\Gamma^{\text{slow}}(I)$ is ~3. Inset: schematic of the decay process of charged biexcitons and charged excitons. (b) The rate Γ^{fast} is calculated from experimental rate Γ^{slow} by assuming that the slope of the SE rate vs intensity curve is proportional to the energy transfer rate of individual QD, as predicted by Eq. (2). (c) The photoluminescence as a function of excitation intensity shows that the emission spectrum retains the plasmon line shape as the peak emission wavelength is ~631 nm.

The experimentally measured SE rate $\Gamma^{\mathrm{Exp}}(I)$ below saturation for QDs participating in CET is given by

$$\Gamma^{\mathrm{Exp}}(I) = \Gamma^{\mathrm{ET}} + \alpha\Gamma^{\mathrm{ET}} I, \tag{1}$$

where the second term represents the cooperative energy transfer rate in the CET intensity range. For weak excitation intensities, i.e., few emitters are excited, cooperative effects are weak and the experimentally measured SE rate Γ^{Exp} should equal individual QD energy transfer rate Γ^{ET}. Equation (1) holds for both fast and slow rates. Accordingly, the ratio of the experimentally measured Γ^{fast} and Γ^{slow} rates from the PNC is

$$\Gamma^{\mathrm{fast}}(I)/\Gamma^{\mathrm{slow}}(I) = (\Gamma^{\mathrm{fast}}_{\mathrm{ET}} + \alpha_{\mathrm{fast}}\Gamma^{\mathrm{fast}}_{\mathrm{ET}} I)/(\Gamma^{\mathrm{slow}}_{\mathrm{ET}} + \alpha_{\mathrm{slow}}\Gamma^{\mathrm{slow}}_{\mathrm{ET}} I), \tag{2}$$

where α_{fast} and α_{slow} are the intensity scaling factors for fast and slow energy transfer rate, respectively. The rates ratio $\Gamma^{\mathrm{fast}}(I)/\Gamma^{\mathrm{slow}}(I)$ for different intensities is ~3 [Fig. 4(a)], which can only be true if $\alpha_{\mathrm{fast}} \approx \alpha_{\mathrm{slow}} \approx \alpha$. Since we have two equations and one unknown, α, we can quantitatively validate our analysis using the measured slow rate $\Gamma^{\mathrm{slow}}(I) = \Gamma^{\mathrm{slow}}_{\mathrm{ET}} + \alpha\Gamma^{\mathrm{slow}}_{\mathrm{ET}} I$, to calculate α to reproduce the experimentally measured fast rate $\Gamma^{\mathrm{fast}} = \Gamma^{\mathrm{fast}}_{\mathrm{ET}} + +\alpha\Gamma^{\mathrm{fast}}_{\mathrm{ET}} I$. Figure 4(b) shows the close agreement between calculated vs measured Γ^{fast}, indicating that the slope of SE rate intensity dependence is proportional $\Gamma^{\mathrm{fast}}_{\mathrm{ET}}$, as predicted by the CET mechanism. For relatively higher intensities, the rate ratio $\Gamma^{\mathrm{fast}}/\Gamma^{\mathrm{slow}}$ exceeds 3 likely because excitons saturate at lower intensities compared to biexcitons [39]. The analysis presented in Figs. 4(a) and 4(b) for a different PNC is shown in the Supplemental Material [24], Fig. S8 to confirm our observation reproducibility.

Figure 4(c) shows the photoluminescence from a PNC vs excitation intensity. The photoluminescence spectrum retains the plasmon resonance central frequency and overall line shape while its amplitude increases linearly with excitation power implying that radiation emanates from the PNC following CET [18]. This is in contrast to superradiance where radiation emanates directly from QEs and changes in the decay rates affect the emission spectra [21]. Furthermore, we exclude stimulated emission and photothermal effects as a cause of SE rate intensity dependence (Supplemental Material [24], Fig. S9).

CET represents an additional degree of freedom to control SE beyond the plasmon-enhanced local field [7]. We used a low Q antenna to ensure that the collected photoluminescence is from the PNC. Future works can use high Q and low V nanoantennas [4] to enhance the SE rate beyond the stimulated emission rate (>100 GHz) which would enable high-speed short-distance optical communication, and enhancing light sources efficiency [6,40,41] (Supplemental Material [24], Fig. S10). Accelerating QDs SE rate can increase the QDs quantum yield by overcoming Auger recombination [42,43]. The demonstrated SE rate-based optical modulator, after overcoming the photobleaching problem, can be used as a multiplexing technique to encode information in the emission rate (Supplemental Material [24], note **2.12**).

The authors would like to thank Eugenio Calandrini for his help with sample preparation. G. S. received funding from the Ohio Third Frontier Project 'Research Cluster on Surfaces in Advanced Materials (RC-SAM) at Case Western Reserve University' and the GU Malignancies Program of the Case Comprehensive Cancer Center and he was supported in part by the National Science Foundation under Grant No. DMR-1708742. J. B. received support from U.S. Department of Energy, Office of Science, Basic Energy Sciences, under Award No. DE-SC008148. T. V. S. was supported in part by the National Science Foundation under Grants No. DMR-1610427, No. DMR-1826886, and No. HRD-1547754. M. E., T. V. S., and G. S. conceived the idea. F. D. A. and E. M. designed and fabricated the samples. M. E., J. B., and G. S. designed the experiments. M. E., A. F., M. W., and E. H. performed the experiments. A. B. and M. E. performed the simulations. M. E. wrote the manuscript with inputs from all the authors. T. V. S., J. B., F. D. A., and G. S. supervised the research. All authors analyzed and discussed the data.

*Corresponding author.
mke23@case.edu
†Corresponding author.
gxs284@case.edu

[1] P. Lodahl, A. Floris van Driel, I. S. Nikolaev, A. Irman, K. Overgaag, D. Vanmaekelbergh, and W. L. Vos, Controlling the dynamics of spontaneous emission from quantum dots by photonic crystals, Nature (London) **430**, 654 (2004).
[2] M. Pelton, Modified spontaneous emission in nanophotonic structures, Nat. Photonics **9**, 427 (2015).
[3] E. M. Purcell, H. C. Torrey, and R. V. Pound, Resonance absorption by nuclear magnetic moments in a solid, Phys. Rev. **69**, 37 (1946).
[4] G. M. Akselrod, C. Argyropoulos, T. B. Hoang, C. Ciracì, C. Fang, J. Huang, D. R. Smith, and M. H. Mikkelsen, Probing the mechanisms of large Purcell enhancement in plasmonic nanoantennas, Nat. Photonics **8**, 835 (2014).
[5] M. El Kabbash, A. Rahimi Rashed, K. V. Sreekanth, A. De Luca, M. Infusino, and G. Strangi, Plasmon-Exciton Resonant Energy Transfer: Across Scales Hybrid Systems, J. Nanomater. **21**, 4819040 (2016).
[6] M. S. Eggleston, K. Messer, L. Zhang, E. Yablonovitch, and M. C. Wu, Optical antenna enhanced spontaneous emission, Proc. Natl. Acad. Sci. U.S.A. **112**, 1704 (2015).
[7] C. Ciracì, R. T. Hill, J. J. Mock, Y. Urzhumov, A. I. Fernández-Domínguez, S. A. Maier, J. B. Pendry, A. Chilkoti, and D. R. Smith, Probing the Ultimate Limits of Plasmonic Enhancement, Science **337**, 1072 (2012).

[8] N. A. Mortensen, S. Raza, M. Wubs, T. Søndergaard, and S. I. Bozhevolnyi, A generalized non-local optical response theory for plasmonic nanostructures, Nat. Commun. **5**, 3809 (2014).
[9] T. V. Shahbazyan, Local Density of States for Nanoplasmonics, Phys. Rev. Lett. **117**, 207401 (2016).
[10] J. J. Choquette, K.-P. Marzlin, and B. C. Sanders, Superradiance, subradiance, and suppressed superradiance of dipoles near a metal interface, Phys. Rev. A **82**, 023827 (2010).
[11] P. A. Huidobro, A. Y. Nikitin, C. González-Ballestero, L. Martín-Moreno, and F. J. García-Vidal, Superradiance mediated by graphene surface plasmons, Phys. Rev. B **85**, 155438 (2012).
[12] D. Martín-Cano, L. Martín-Moreno, F. J. García-Vidal, and E. Moreno, Resonance energy transfer and superradiance mediated by plasmonic nanowaveguides, Nano Lett. **10**, 3129 (2010).
[13] V. N. Pustovit and T. V. Shahbazyan, Cooperative Emission of Light by an Ensemble of Dipoles Near a Metal Nanoparticle: The Plasmonic Dicke Effect, Phys. Rev. Lett. **102**, 077401 (2009).
[14] V. N. Pustovit and T. V. Shahbazyan, Plasmon-mediated superradiance near metal nanostructures, Phys. Rev. B **82**, 075429 (2010).
[15] R. Bonifacio and L. A. Lugiato, Cooperative radiation processes in two-level systems: Superfluorescence, Phys. Rev. A **11**, 1507 (1975).
[16] K. Cong, Q. Zhang, Y. Wang, G. T. Noe, A. Belyanin, and J. Kono, Dicke superradiance in solids [Invited], J. Opt. Soc. Am. B **33**, C80 (2016).
[17] M. V. Shestakov, E. Fron, L. F. Chibotaru, and V. V. Moshchalkov, Plasmonic Dicke effect in Ag-nanoclusters-doped oxyfluoride glasses, J. Phys. Chem. C **119**, 20051 (2015).
[18] T. V. Shahbazyan, Cooperative emission mediated by cooperative energy transfer to a plasmonic antenna, Phys. Rev. B **99**, 125143 (2019).
[19] L. Novotny and B. Hecht, *Principles of Nano-Optics* (Cambridge University Press, Cambridge, England, 2006).
[20] R. Friedberg, S. R. Hartmann, and J. T. Manassah, Frequency shifts in emission and absorption by resonant systems ot two-level atoms, Phys. Rep. **7**, 101 (1973).
[21] M. Gross and S. Haroche, Superradiance: An essay on the theory of collective spontaneous emission, Phys. Rep. **93**, 301 (1982).
[22] R. H. Dicke, Coherence in spontaneous radiation processes, Phys. Rev. **93**, 99 (1954).
[23] M. Scheibner, T. Schmidt, L. Worschech, A. Forchel, G. Bacher, T. Passow, and D. Hommel, Superradiance of quantum dots, Nat. Phys. **3**, 106 (2007).
[24] See Supplemental Material at http://link.aps.org/supplemental/10.1103/PhysRevLett.122.203901for further details, which includes Refs. [25–30].
[25] T. Wang, S. F. Yelin, R. Côté, E. E. Eyler, S. M. Farooqi, P. L. Gould, M. Koštrun, D. Tong, and D. Vrinceanu, Superradiance in ultracold Rydberg gases, Phys. Rev. A **75**, 033802 (2007).
[26] P. E. Lippens and M. Lannoo, Comparison between calculated and experimental values of the lowest excited electronic state of small CdSe crystallites, Phys. Rev. B **41**, 6079 (1990).
[27] M. A. Young, J. A. Dieringer, and R. P. Van Duyne, in *Tip Enhancement*, edited by S. Kawata and V. M. Shalaev (Elsevier, Amsterdam, 2007), p. 1.
[28] J. B. Khurgin, How to deal with the loss in plasmonics and metamaterials, Nat. Nanotechnol. **10**, 2 (2015).
[29] S. Cueff, D. Li, Y. Zhou, F. J. Wong, J. A. Kurvits, S. Ramanathan, and R. Zia, Dynamic control of light emission faster than the lifetime limit using VO2 phase-change, Nat. Commun. **6**, 8636 (2015).
[30] Y.-J. Lu, R. Sokhoyan, W.-H. Cheng, G. Kafaie Shirmanesh, A. R. Davoyan, R. A. Pala, K. Thyagarajan, and H. A. Atwater, Dynamically controlled Purcell enhancement of visible spontaneous emission in a gated plasmonic heterostructure, Nat. Commun. **8**, 1631 (2017).
[31] C.-Y. Jin, R. Johne, M. Y. Swinkels, T. B. Hoang, L. Midolo, P. J. van Veldhoven, and A. Fiore, Ultrafast non-local control of spontaneous emission, Nat. Nanotechnol. **9**, 886 (2014).
[32] F. Pagliano, Y. Cho, T. Xia, F. van Otten, R. Johne, and A. Fiore, Dynamically controlling the emission of single excitons in photonic crystal cavities, Nat. Commun. **5**, 5786 (2014).
[33] C. Ryan *et al.*, Roll-to-roll fabrication of multilayer films for high capacity optical data storage, Adv. Mater. **24**, 5222 (2012).
[34] F. De Angelis, M. Malerba, M. Patrini, E. Miele, G. Das, A. Toma, R. P. Zaccaria, and E. Di Fabrizio, 3D hollow nanostructures as building blocks for multifunctional plasmonics, Nano Lett. **13**, 3553 (2013).
[35] M. Malerba *et al.*, 3D vertical nanostructures for enhanced infrared plasmonics, Sci. Rep. **5**, 16436 (2015).
[36] M. P. G. W. Bryant, *Introduction to Metal-Nanoparticle Plasmonics* (Wiley, 2013).
[37] M. Ringler, A. Schwemer, M. Wunderlich, A. Nichtl, K. Kürzinger, T. A. Klar, and J. Feldmann, Shaping Emission Spectra of Fluorescent Molecules with Single Plasmonic Nanoresonators, Phys. Rev. Lett. **100**, 203002 (2008).
[38] N. Hiroshige, T. Ihara, and Y. Kanemitsu, Simultaneously measured photoluminescence lifetime and quantum yield of two-photon cascade emission on single CdSe/ZnS nanocrystals, Phys. Rev. B **95**, 245307 (2017).
[39] K. Matsuzaki *et al.*, Strong plasmonic enhancement of biexciton emission: Controlled coupling of a single quantum dot to a gold nanocone antenna, Sci. Rep. **7**, 42307 (2017).
[40] J. S. Biteen, D. Pacifici, N. S. Lewis, and H. A. Atwater, Enhanced radiative emission rate and quantum efficiency in coupled silicon nanocrystal-nanostructured gold emitters, Nano Lett. **5**, 1768 (2005).
[41] K. Tsakmakidis, In the limelight, Nat. Mater. **11**, 1000 (2012).
[42] S. Gupta and E. Waks, Overcoming Auger recombination in nanocrystal quantum dot laser using spontaneous emission enhancement, Opt. Express **22**, 3013 (2014).
[43] T. B. Hoang, G. M. Akselrod, C. Argyropoulos, J. Huang, D. R. Smith, and M. H. Mikkelsen, Ultrafast spontaneous emission source using plasmonic nanoantennas, Nat. Commun. **6**, 7788 (2015).